Proceedings of the 17th World Congress
The International Federation of Automatic Control
Seoul, Korea, July 6-11, 2008

Local orbital frame predictor for LEO drag-free satellite

Enrico Canuto* Luca Massotti**

**Politecnico di Torino, Dipartimento di Automatica e Informatica*
Corso Duca degli Abruzzi 24, 10129 Torino, Italy(e-mail: enrico.canuto@polito.it)
***ESA Earth Observation Future Missions Division,*
ESTEC EOP-SF, Noordwijk NL-220 AG, The Netherlands(e-mail: luca.massotti@esa.int)

Abstract: This paper is concerned with on-board real-time position and rate prediction of the spacecraft centre-of-mass as input data to local orbital frame (LORF) determination for Low-Earth Orbit drag-free satellites. Study and simulation results are justified by Drag-Free and Attitude Control of the GOCE satellite (Gravity field and steady-state Ocean Circulation Explorer), the LORF being the instantaneous reference for satellite attitude and scientific data. The paper focuses on modeling issues to obtain an accurate orbit dynamics at lower frequencies for reducing integration error because of the narrow-band filter requested by the assumed wide-band measurement errors. A further remedy in this sense is the addition of a second order disturbance dynamics leaving unexplained bounded noise components. Simulated results are presented with reference to GOCE mission.

1. INTRODUCTION

This paper is concerned with on-board real-time position and rate determination of the spacecraft centre-of-mass (CoM) as input data to local orbital frame (LORF) determination for LEO (Low-Earth Orbit) drag-free satellites. Study and simulation results are justified by Drag-Free and Attitude Control of the GOCE satellite (Gravity field and steady-state Ocean Circulation Explorer), the LORF being the instantaneous reference for satellite attitude and scientific data (Canuto *et al.,* 2003, Canuto, 2007b and 2007c). Accuracy requirements directly descend from attitude and lead to microradian errors in the so-called mission Measurement Bandwidth (MBW) from 1 mHz to 0.1 Hz to be compared with an overall sub-milliradian error range, because of relaxed low-frequency attitude below 1 mHz.

The LORF provides the orientation of the osculating instantaneous orbit with respect to an inertial frame as the Equatorial Earth centered at some date or with respect to a mean Earth-fixed circular orbit only determined by mean Earth gravity, being the satellite drag-free. In the latter case, Euler angles of the LORF-to-mean orbit transformation can be shown to be combination of the ratios between CoM position and rate perturbations with respect to the mean orbit radius and the absolute orbital speed. Direct LORF determination in the order of microradian would imply CoM position and rate measurement errors below few meters and 1 cm/s , respectively, at a sampling rate greater than 0.1 Hz. Although space-borne GPS receivers approach this limits at a sampling rate of 1 Hz, position and rate measurements need be filtered to cope with non-stationary GPS errors and to extrapolate measurements during sampling time as requested by higher control rates above 1 Hz. The objective is to dispose of a robust algorithm, free of measurement statistics, and tuned to quite conservative GPS errors as shown in Table 1.

Table 1. GPS timing and errors

Parameter	Unit	Value
Sampling time	s	1
Position error	m	<30 (1σ)
Rate error	m/s	0.03 (1σ)
Bias		negligible
Delay		negligible

On-board GPS data have been extensively used for several purposes: among them, real-time and a-posteriori orbit determination (Montenbruck and Gill, 2000), attitude determination, relative positioning and time synchronization. A survey can be found in Bisnath, 2004.

2. REFERENCE FRAMES AND REQUIREMENTS

The inertial frame $\mathcal{R}_J = \{O, \mathbf{i}_J, \mathbf{j}_J, \mathbf{k}_J\}$ centered in the Earth CoM O, is the equatorial frame at the date J2000. The LORF $\mathcal{R}_O = \{C, \mathbf{i}_O, \mathbf{j}_O, \mathbf{k}_O\}$, centered in the spacecraft CoM C, is defined by the instantaneous orbit orientation, and specifically by the motion direction $\mathbf{v}/|\mathbf{v}|$ of the CoM, $\mathbf{v}$ being the inertial velocity, and by the orbital plane orthogonal to the angular momentum $\mathbf{h} = m_s \mathbf{r} \times \mathbf{v}$, m_s denoting spacecraft mass and $\mathbf{r}$ CoM position (Fig. 1). The LORF is the reference frame for science measurements and attitude control. The LORF axes are defined by

$$\mathbf{i}_O = \mathbf{v}/|\mathbf{v}|, \mathbf{j}_O = \mathbf{r} \times \mathbf{v}/|\mathbf{r} \times \mathbf{v}|, \mathbf{k}_O = \mathbf{i}_O \times \mathbf{j}_O \qquad (1)$$

The axes from $\mathbf{i}_O$ to $\mathbf{k}_O$, are referred to as along-track, out-of-plane and radial, respectively.

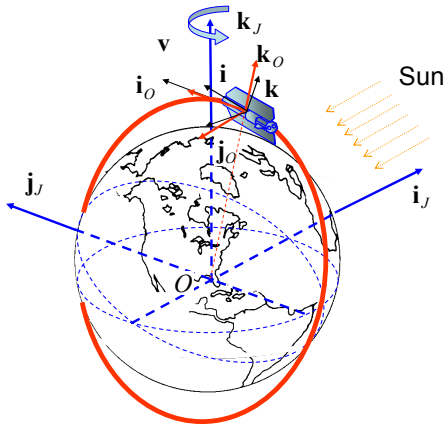

Fig. 1. LEO sun-synchronous orbit and reference frames.

The matrix $\mathbf{R}_O = [\mathbf{i}_O \quad \mathbf{j}_O \quad \mathbf{k}_O]$ accomplishes the LORF-to-inertial coordinate transformation, and defines the reference attitude to be tracked by the spacecraft. Assuming a quasi-circular circular orbit, the orientation error $\mathbf{e}_O$, caused by the on-line estimate $\hat{\mathbf{R}}_O$, (2)can be shown to be related to inertial position and velocity estimation errors $\Delta\mathbf{r}$ and $\Delta\mathbf{v}$ through

$$\mathbf{e}_O \cong \frac{1}{\underline{r}} \begin{vmatrix} -\Delta\mathbf{r}\cdot\mathbf{j}_O \\ \Delta\mathbf{r}\cdot\mathbf{i}_O - \Delta\mathbf{v}\cdot\mathbf{k}_O/\underline{\omega}_O \\ \Delta\mathbf{v}\cdot\mathbf{j}_O/\underline{\omega}_O \end{vmatrix}, \underline{r} = \|\mathbf{r}\|,\ \underline{v} = \underline{\omega}_O\underline{r} = \|\mathbf{v}\|, \qquad (3)$$

where $\underline{\omega}_O = \sqrt{\mu/\underline{r}^3} \simeq 1.2$ mrad/s is the mean orbital rate at geodetic height $h = 250$ km.

Assume now LORF matrix to be directly measured from GPS measurements

$$\begin{aligned} \mathbf{y}_r(t_j) &= \mathbf{r}(t_j) + \mathbf{v}_r(t_j) \\ \mathbf{y}_v(t_j) &= \mathbf{v}(t_j) + \mathbf{v}_v(t_j),\ t_j = jT_g \end{aligned}, \qquad (4)$$

which are collected from GPS at uniform sampling rate $f_g = 1/T_g = 1$ Hz. Properties of GPS errors $\mathbf{v}_r$ and $\mathbf{v}_v$ are not recalled here (see Kaplan, 1996), but they are assumed to be discrete-time white and Gaussian noise, and their components to be statistically independent. Assume position and rate errors to be bounded as in Table 2, and denoted their standard deviations with σ_r and σ_v, respectively. Then, assuming the equality

$$\Delta\mathbf{r}(t_j) = \mathbf{v}_r(t_j),\ \Delta\mathbf{v}(t_j) = \mathbf{v}_v(t_j) \qquad (5)$$

in (3), yields the white noise PSD

$$\begin{vmatrix} S_{Ox} \\ S_{Oy} \\ S_{Oz} \end{vmatrix}(f) \cong \frac{\sqrt{2T_g}}{r} \begin{vmatrix} \sigma_r \\ \sqrt{\sigma_r^2 + (\sigma_v/\underline{\omega}_O)^2} \\ \sigma_v/\underline{\omega}_O \end{vmatrix} \le \begin{vmatrix} 6.5 \\ 8.5 \\ 5.5 \end{vmatrix} \frac{\mu\text{rad}}{\sqrt{\text{Hz}}} \qquad (6)$$

$$|f| \le 0.5 f_g = 0.5\text{Hz}$$

for each LORF component error. The acronym PSD means the root of the unilateral power spectral density, throughout.

Requirements to LORF estimation errors come from spacecraft attitude as the latter is defined by the body-to-LORF transformation. LORF errors should be a fraction of the residual attitude as shown in Table 2, derived from the GOCE requirements.

Table 2. Bounds to LORF errors and attitude

Variable	Overall RMS [μrad]	MBW PSD $\left[\mu\text{rad}/\sqrt{\text{Hz}}\right]$
LORF error	200	4.3
Attitude	370	7.9

The most stringent requirements in Table 2 occur in the so-called MBW from 1 mHz to 0.1 Hz. The direct LORF measurement, being not compliant according to (6), justifies a real-time filter guaranteeing requirements with some margin. The filter will be designed in the form a state observer around a stylized discrete-time dynamics called Embedded Model, as suggested by Canuto (2004, 2007a).

3. EMBEDDED MODEL

First, orbit dynamics is derived in continuous-time. An alternative is to use local coordinates with respect to a circular orbit, which provides a version of Hill's equation (Canuto, 2007b); this way is not pursued here. The discrete-time model is derived for each inertial coordinate by exploiting their weak interaction due to quasi-circular orbit and quasi-spherical gravity field.

3.1 Orbit dynamics

Assume the LEO satellite is free-falling, i.e. a drag-free control cancels non-gravitational forces below a certain threshold. Denote the residual non gravitational CoM acceleration, ideally held to zero, with $\mathbf{a}$. The inertial position $\mathbf{r}^T = [x \quad y \quad z]^T$, is related to the Earth-fixed coordinates (7) through longitude λ and latitude θ. Denote the Earth's gravitational potential with $U(r,\lambda,\theta)$, which is usually expanded into complex spherical harmonics $\bar{Y}_{nm}(\theta,\lambda)$ of degree n and order m, scaled by the complex spectrum $\bar{K}_{nm}$. The fine structure of fluctuations according to Kaula (Bertotti and Farinella, 1990) mainly depends on the degree n and is approximated by the so-called Kaula's rule

$$K_n \simeq 10^{-5} n^{-2},\ n >> 1,\ K_n = \sqrt{(2n+1)\sum_{m=-n}^{n} \left|\bar{K}_{nm}\right|^2}. \qquad (8)$$

By holding the spherical term and the 2nd order term due to Earth flatness in the U expansion and by confining higher order terms into a single anomaly δU, one obtains

$$U(r,z) = \frac{\mu}{r}\left(1 - \frac{3}{2}J_2\left(\frac{R}{r}\right)^2\left(\left(\frac{z}{r}\right)^2 - \frac{1}{3}\right)\right) + \delta U, \qquad (9)$$

where $J_2 \simeq 0.001$ and the explicit term is independent of the Earth's rotation.

The gravity acceleration $\mathbf{g} = \nabla U$ is derived from (9), the explicit component being expressed into inertial coordinates as follows

$$\mathbf{g} = -\frac{\mu}{r^3}\left(I - \frac{3J_2}{2}\left(\frac{R}{r}\right)^2\left(5\left(\frac{z}{r}\right)^2 I - \Gamma\right)\right)\mathbf{r} + \delta\mathbf{g}, \qquad (10)$$

where $\Gamma = \mathrm{diag}\{1,1,3\}$ and the anomaly $\delta\mathbf{g}(\mathbf{r})$ corresponds to δU.

A further simplification comes by assuming a quasi circular orbit as in GOCE. The explicit terms in (10) are expanded around $\underline{r}$ with the care of keeping perturbation terms of the same order of magnitude as J_2 and of confining residuals into $\delta\mathbf{g}(\mathbf{r})$. This amounts to 1st order expanding the spherical term and to zero-th order expanding the flatness terms, which gives the final expression

$$\begin{aligned}\mathbf{g}(\mathbf{r}(t)) &= -\underline{\omega}_O^2\left(I+\partial\Omega(\mathbf{r})\right)\mathbf{r}(t)+\delta\mathbf{g}(\mathbf{r})\\ \partial\Omega(\mathbf{r}) &= 3(1-r/\underline{r})I+\gamma_0(z/\underline{r})^2 I-\Gamma_1\\ \gamma_0 &= \frac{15}{2}J_2(R/\underline{r})^2,\ \Gamma_1=\frac{3}{2}J_2(R/\underline{r})^2\Gamma\end{aligned}. \quad (11)$$

The perturbation term $\partial\Omega(\mathbf{r})$ of the orbit rate in (11), which is clearly bounded by

$$\left|\partial\Omega(\mathbf{r})\right| \le 3(\varepsilon+2J_2) \simeq 0.015, \quad (12)$$

is assumed to be periodic in time and possess a long-term average. Eccentricity and flatness contributing by the same order of magnitude justify (11). Higher order terms contribute to less than 0.0001.

Orbit dynamics can then be written as

$$\begin{aligned}\begin{bmatrix}\dot{\mathbf{r}}\\ \dot{\mathbf{v}}\end{bmatrix}(t) &= \begin{bmatrix}0 & I\\ -\underline{\omega}_O^2\left(I+\partial\Omega(\mathbf{r})\right) & 0\end{bmatrix}\begin{bmatrix}\mathbf{r}\\ \mathbf{v}\end{bmatrix}(t)+\begin{bmatrix}0\\ I\end{bmatrix}\mathbf{a}_d(t)\\ \mathbf{a}_d(t) &= \mathbf{a}(t)+\delta\mathbf{g}(t)\end{aligned}, \quad (13)$$

having combined the residual non-gravitational acceleration and gravity anomalies into $\mathbf{a}_d$. CoM coordinates in (13) are each other connected through the weak perturbing term $\partial\Omega(\mathbf{r})$.

3.2 Discrete-time dynamics

Embedded model according to Canuto, (2004, 2007a) is made by two interconnected parts: the controllable dynamics and the disturbance dynamics. The orbit being drag-free the input to controllable part is assumed to be quasi-zero except for gravity acceleration. The latter is partitioned into a position feedback to be part of the controllable dynamics and residual components treated as an unknown disturbance driven by arbitrary signals.

Consider a time unit $T = T_g/n$, with $n_g \ge 1$ and assume $T << T_O = 2\pi/\underline{\omega}_O$, which implies (13) to be LTI during T and the discrete-time version to become time varying. The generic discrete time will denoted by $t_i = iT$. We shall limit to a single generic CoM coordinate $r_k, k = 1,2,3$ with increment v_k [m], collected into the state $\mathbf{x}_k^T = [r_k \quad v_k]$. To this end, denote the angular increment associated to r_k with $\alpha_{ki} = \omega_{ki}T$, where

$$\mathrm{diag}\{\alpha_{1i}^2, \alpha_{2i}^2, \alpha_{3i}^2\} = \underline{\omega}_O^2 T^2\left(I+\partial\Omega(\mathbf{r}(t_i))\right). \quad (14)$$

The discrete-time equation holds

$$\begin{aligned}\begin{bmatrix}r_k\\ v_k\end{bmatrix}(i+1) &= \begin{bmatrix}\cos\alpha_{ki} & \frac{\sin\alpha_{ki}}{\alpha_{ki}}\\ -\alpha_{ki}\sin\alpha_{ki} & \cos\alpha_{ki}\end{bmatrix}\begin{bmatrix}r_k\\ v_k\end{bmatrix}(i)+\\ &+\int_{t_i}^{t_{i+1}}\begin{bmatrix}\frac{\sin(\omega_{ki}(t_{i+1}-\tau))}{\omega_{ki}}\\ T\cos(\omega_{ki}(t_{i+1}-\tau))\end{bmatrix}a_{dk}(\tau)\,d\tau\end{aligned} \quad (15)$$

where a_{dx} is a coordinate of $\mathbf{a}_d$.

By exploiting $T << T_O$, (15) can be further simplified for real-time computation by replacing trigonometric functions with polynomial expansions up to 2nd order terms in α_{ki}, which yields

$$\begin{aligned}\begin{bmatrix}r_k\\ v_k\end{bmatrix}(i+1) &= \begin{bmatrix}1-\alpha_{ki}^2/2 & 1-\alpha_{ki}^2/6\\ -\alpha_{ki}^2 & 1-\alpha_{ki}^2/2\end{bmatrix}\begin{bmatrix}r_k\\ v_k\end{bmatrix}(i)+\\ &+\int_{t_i}^{t_{i+1}}\begin{bmatrix}(t_{i+1}-\tau)I\\ T\end{bmatrix}a_{dk}(\tau)\,d\tau\end{aligned}. \quad (16)$$

Integration in (16) is solved (i) by defining a disturbance increment $d_k(i)$, in length units [m], holding

$$d_k(i) = T\int_{t_i}^{t_{i+1}} a_{dk}(\tau)\,d\tau, \quad (17)$$

and (ii) by dropping the direct effect of a_{dk} on $v_k(i) = r_k(i+1) - r_k(i)$, as the former just corresponds to time integration of the unique disturbance source $d_k(i)$. The result is the discrete-time version of a time-varying oscillator having very long period with respect to time unit T and subject to an acceleration disturbance:

$$\begin{aligned}\mathbf{x}_k(i+1) &= A_{ck}(i)\mathbf{x}_{xk}(i)+B_c d_k(i)\\ A_{ck}(i) &= \begin{bmatrix}1-\alpha_{ki}^2/2 & 1-\alpha_{ki}^2/4\\ -\alpha_{ki}^2 & 1-\alpha_{ki}^2/2\end{bmatrix},\ B_c = \begin{bmatrix}0\\ 1\end{bmatrix}.\end{aligned} \quad (18)$$

Note $A_{ck}(i)$ is slowly time-varying with the orbit angular increment α_{ki} and has eigenvalues slightly off the unit circle, but they will be stabilized by the state predictor. The LORF predictor (Section 4.) is designed to have steady eigenvalues through time-varying feedback gains. Equation (18) must be completed with the disturbance dynamics as below.

Disturbance dynamics is synthesized starting from the experimental PSD of the CoM disturbances (Canuto, 2007a, 2007c). (i) Residual non-gravitational acceleration are retained a wide-band noise within the performance BW. The wide-band noise is modelled as a white noise w_{0k}. Drifts due to accelerometers are included in the gravity anomaly dynamics as follows. (ii) Gravity anomalies and the modeling errors of the spherical and J2 terms are modelled from the spectral density of the gravity anomalies rolling off at -40dB/dec beyond the 3rd orbit harmonics as shown in Fig. 2. To this end, the total disturbance d_k is decomposed into the sum of white noise w_{0x} and the combination of random drifts $\mathbf{z}_k^T = [z_{1k} \quad z_{2k}]$, driven by a pair of white noise w_{1k} and w_{2k}, which are collected together with w_{0k} into $\mathbf{w}_k$.

Disturbance dynamics, to be repeated for each coordinate, is

$$\begin{aligned}\mathbf{z}_k(i+1) &= A_d\mathbf{z}_k(i) + G_d\mathbf{w}_k(i)\\ B_c d_k(i) &= H_c\mathbf{z}_k(i) + G_c\mathbf{w}_k(i)\end{aligned}, \tag{19}$$

and the relevant matrices hold

$$A_d = \begin{bmatrix}1 & 1\\ 0 & 1\end{bmatrix}, G_d = \begin{bmatrix}0 & 1 & 0\\ 0 & 0 & 1\end{bmatrix}, H_c = \begin{bmatrix}0 & 0\\ 1 & 0\end{bmatrix}, G_c = \begin{bmatrix}0 & 0 & 0\\ 1 & 0 & 0\end{bmatrix}. \tag{20}$$

Dynamics (19) is in agreement with Kaula's rule since the Fourier frequency f [Hz] is related to n by

$$f = n\underline{\omega}_O/(2\pi) = n\underline{f}_O \simeq 0.19n, \tag{21}$$

which implies the time profiles of the Earth's gravity accelerations to show a PSD rolling off at -40 dB/dec just after resonances at the 1st and 3rd orbit harmonics due to J2 terms. (22)Fig. 2 shows the PSD of the gravity acceleration anomalies in J2000 coordinates obtained from measured coefficients up to degree $n = 36$ and stochastic extrapolation up to 1 Hz from Kaula's rule. Fig. 2 fully confirms the adopted model.

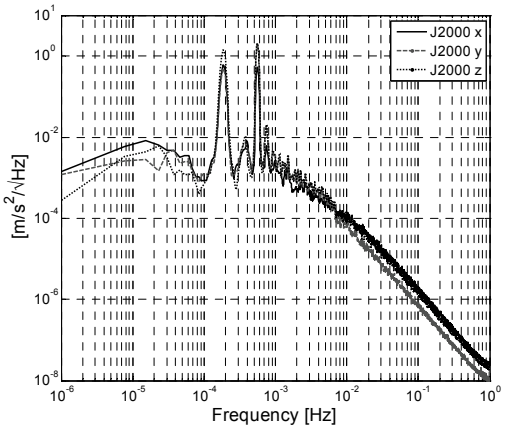

Fig. 2. PSD of the gravity acceleration anomalies.

3.3 Embedded model and model error

The complete model of a single coordinate is the combination of (18) and (19), and is rewritten below by dropping subscript k and adding subscript m, which stands for model:

$$\begin{bmatrix}\mathbf{x}_m\\ \mathbf{z}_m\end{bmatrix}(i+1) = F\begin{bmatrix}\mathbf{x}_m\\ \mathbf{z}_m\end{bmatrix}(i) + G\mathbf{w}(i),\ \mathbf{y}_m(i) = C\begin{bmatrix}\mathbf{x}_m\\ \mathbf{z}_m\end{bmatrix}(i)$$
$$F = \begin{bmatrix}A_c(i) & H_c\\ 0 & A_d\end{bmatrix}, G = \begin{bmatrix}G_c\\ G_d\end{bmatrix} C = \begin{bmatrix}I & 0\end{bmatrix} \tag{23}$$

Note $A_c(i) = A_c(\mathbf{r}_m(i))$ depends on the state itself through the perturbing term α_i^2 rewritten from (14) as

$$\alpha_i^2 = \underline{\alpha}_0^2\left(1 + \partial\Omega(\mathbf{r}_m(i))\right). \tag{24}$$

Equation size is denoted by

$$\begin{aligned}n_y &= \dim\mathbf{y}_m = 2,\ n_w = \dim\mathbf{w} = 3\\ n_c &= \dim\mathbf{x} = 2,\ n_d = \dim\mathbf{z} = 2\end{aligned}. \tag{25}$$

Denote the sampled measurements from GPS receiver with $\mathbf{y}(i)$. They are related to $\mathbf{y}_m$ by the model error $\mathbf{e} = \mathbf{y} - \mathbf{y}_m$, which according to Canuto (2007a) is the composition of a neglected dynamics $\partial\mathbf{P}(\mathbf{y}_m,...)$ in fractional form and of a residual noise $\mathbf{v}$ including GPS errors. The model error relation is written as

$$\mathbf{y}(i) = \mathbf{y}_m(i) + \partial\mathbf{P}(\mathbf{y}_m,...) + \mathbf{v}(i). \tag{26}$$

An expression of $\partial\mathbf{P}(\cdot)$ can be derived from (15), (23) and (26) upon definition of the following errors

$$\mathbf{e}_x(i) = \mathbf{x}(i) - \mathbf{x}_m(i),\ \mathbf{e}_d(i) = \mathbf{a}(i) - B_c d(i). \tag{27}$$

The state equation is written as

$$\begin{aligned}\mathbf{e}_x(i+1) &= A(\mathbf{r})\mathbf{e}_x(i) + \left(A(\mathbf{r}) - A_c(\mathbf{r}_m)\right)\mathbf{y}_m(i) + \mathbf{e}_d(i)\\ \mathbf{e}(i) &= \mathbf{e}_x(i) + \mathbf{v}(i)\end{aligned}, \tag{28}$$

where $A(\mathbf{r})$ is the state matrix in (15) and the input matrix driven by $\mathbf{y}_m$ can be expanded as

$$A(\mathbf{r}) - A_c(\mathbf{r}_m) = \delta A_0 \nabla\alpha_i^2(\underline{\mathbf{r}})(\mathbf{r} - \mathbf{r}_m)(i) + \delta A_1(\mathbf{r}). \tag{29}$$

Expansion coefficients hold

$$\begin{aligned}\delta A_0 &= \begin{bmatrix}-1/2 & -1/4\\ -1 & -1/2\end{bmatrix},\ \delta A_1(\mathbf{r}) = o(\alpha_i^4)\\ \nabla\alpha_i^2(\underline{\mathbf{r}})(\mathbf{r} - \mathbf{r}_m) &\simeq -3\underline{\omega}_O^2 T^2 \underline{r}^{-2}\underline{\mathbf{r}}^T(\mathbf{r} - \mathbf{r}_m)\end{aligned}, \tag{30}$$

with the trick that $\underline{\mathbf{r}}$ is intermediate to $\mathbf{r}$ and $\mathbf{r}_m$ so as to preserve equality in (29).

4. NOISE ESTIMATOR AND STATE OBSERVER

4.1 State prediction

State prediction is strictly related to noise design ending into equation (19). As in Kalman filtering, the model error $\mathbf{e}$ is the source for real-time estimating noise $\mathbf{w}$, or better, some causal combination of past values. Unlike classical predictors where driving noise is acting on each state variable, noise channels in (18) and (19) are respected implying no driving noise to directly perturb the rate v as outlined in Section 3.2. As explained in Canuto (2007a), this constraint may require a dynamic noise estimator when

$$n = n_c + n_d > n_w \times n_y, \tag{31}$$

which is not the present case, as position and rate measurements are available. A static noise estimator applies and holds

$$\bar{\mathbf{w}}(i) = L(i)\bar{\mathbf{e}}(i),\ \bar{\mathbf{e}}(i) = \mathbf{y}(i) - \hat{\mathbf{y}}_m(i), \tag{32}$$

where (i) bar and hat account for estimator inaccuracies to be treated below, (ii) the gain matrix $L(i)$, sized $n_w \times n_y = 6 > n = 4$, is time-varying to force closed-loop dynamics (model and noise estimator) to be LTI.

Since $L(i)$ is oversized with respect to model dynamics, some entries can be forced to zero, while respecting stability. Denote the entries as follows

$$L(i) = \begin{bmatrix}l_{0r} & l_{0v}\\ l_{1r} & l_{1v}\\ l_{2r} & l_{2v}\end{bmatrix}(i), \tag{33}$$

and compute the characteristic polynomial $P(\gamma)$ of the state predictor

$$\begin{bmatrix}\hat{\mathbf{x}}_m\\ \hat{\mathbf{z}}_m\end{bmatrix}(i+1)=\begin{bmatrix}A_c(i)-G_cL(i) & H_c\\ -G_dL(i) & A_d\end{bmatrix}\begin{bmatrix}\hat{\mathbf{x}}_m\\ \hat{\mathbf{z}}_m\end{bmatrix}(i)+ \\ +\begin{bmatrix}G_c\\ G_d\end{bmatrix}L(i)\mathbf{y}(i),\ \hat{\mathbf{y}}_m(i)=\hat{\mathbf{x}}_m(i) \quad (34)$$

Straightforward computation, upon definition of $\gamma=1-\lambda$, λ denoting a generic eigenvalue, yields

$$\begin{aligned}&P(\gamma)=\gamma^4+c_3\gamma^3+c_2\gamma^2+c_1\gamma+c_0\\ &c_3=l_{ov}+\alpha_i^2,\ c_0=\alpha_i^2l_{2v}/2+(1-\alpha_i^2/4)l_{2r}\\ &c_2=l_{1v}+(\alpha_i^2+l_{0r})(1-\alpha_i^2/4)+\alpha_i^2(\alpha_i^2/2+l_{ov})/2\\ &c_1=(1-\alpha_i^2/4)l_{1r}+\alpha_i^2l_{1v}/2+l_{2v}\end{aligned}, \quad (35)$$

where the polynomial coefficients, depending on the closed-loop eigenvalues λ_h, $h=1,\ldots,n$, are constant and show multiple solutions to exist.

To find a unique solution, simplify (35) by provisionally setting $\alpha_i^2=0$, which leads to

$$\begin{aligned}&c_3\simeq l_{ov},\ c_2\simeq l_{1v}+l_{0r}\\ &c_1\simeq l_{2v}+l_{1r},\ c_0\simeq l_{2r}\end{aligned}, \quad (36)$$

and implies four alternatives to exist, if the useless coefficients are set to zero as in Table 3.

Table 3. Noise estimator alternatives

Case	l_{1v}	l_{2v}	l_{0r}	l_{1r}	X means not zero
0	0	0	X	X	Higher noise
1	0	X	X	0	Intermediate
2	X	0	0	X	Intermediate
3	X	X	0	0	Lower noise

Table 3 and (36) show, (i) in the case 3, the rate measurement are capable of estimating all noise components, (ii) the position measurement being necessary to guarantee closed-loop stability as imposed by the last equation in (36).

Since position measurement is much noisier than rate as Table 3 shows, case 3 must be selected as it favours Kalman filter guideline, proper of any measuring strategy, of reducing to a minimum any measurement noise passing through the noise-estimator feedback channels. A formal proof may be provided.

4.2 Predictor-corrector

Actually prediction equation (34) can only be implemented with $L(i)=0$ because of to lower measurement rate $T_g^{-1}<T^{-1}$. This implies conversion to predictor-corrector scheme. Several schemes are possible. Denote with $t_j=jT_g$ the measurement times, such that $t_{i_j}=t_j$ for $i_j=n_gj$. At each time t_j the prediction-correction is invoked

$$\begin{bmatrix}\overline{\mathbf{x}}_m\\ \overline{\mathbf{z}}_m\end{bmatrix}(j)=\begin{bmatrix}\hat{\mathbf{x}}_m\\ \hat{\mathbf{z}}_m\end{bmatrix}(i_j)+\begin{bmatrix}K_c(j)\\ K_d(j)\end{bmatrix}\overline{\mathbf{e}}(i_j), \quad (37)$$

where the variable gains depend on the predictor gain $L(i_j)$ through the following equation

$$\begin{bmatrix}K_c(j)\\ K_d(j)\end{bmatrix}=\begin{bmatrix}A_c(i_j) & H_c\\ 0 & A_d\end{bmatrix}^{-1}\begin{bmatrix}G_c\\ G_d\end{bmatrix}L(i_j). \quad (38)$$

At each step i the predictor (34) is invoked with $L(i)=0$ and initial conditions

$$\hat{\mathbf{x}}_m(i_j)=\overline{\mathbf{x}}_m(j),\ \hat{\mathbf{z}}_m(i_j)=\overline{\mathbf{z}}_m(j). \quad (39)$$

Computing burden due to variable gains may be reduced either by decomposing the gain into steady and variable part, or, more drastically, by reducing (23) to be LTI, which is obtained by treating the variable part of (14) as a known disturbance.

In the above scheme, asymptotic stability of the closed-loop state matrix in (34) is not sufficient to guarantee predictor-corrector stability, since the multi-step prediction matrix holds

$$F_h(j)=F(j)^h\left(F(j)-GL(j)C\right),\ h=0,...,n-1. \quad (40)$$

The drawback may be circumvented by rewriting (35) in terms of the characteristic polynomial of F_n. An alternative scheme, free of stability problems, is to implement (34) each measurement time $t_j=jT_g$ and then interpolate during T_g.

4.3 Stability in presence of model uncertainty

According to (28), the neglected dynamics repeats the 'true' dynamics in (15) less a forcing error depending on $\mathbf{y}_m$ and due to approximate gravitational acceleration. The latter may be in turn interpreted as a structured uncertainty which is treated by the Embedded Model as an unknown disturbance, and therefore is encompassed by disturbance dynamics (19). It can be shown as in Canuto, 2007b, closed-loop stability requests the predictor BW to be larger than a limit frequency $f_{\min}$, which is related to the largest uncertainty on (14). Since the latter is of the order of 0.001 also in case the variable part of (14) is neglected, it results

$$f_{\min}<\underline{f}_O=0.5\underline{\omega}_O/\pi\simeq 0.2\ \text{mHz}. \quad (41)$$

The above inequality is consistent with the BW upper bound imposed by the measurement errors as shown in Section 5.

5. SIMULATED RESULTS

Simulated results concern GOCE mission during 42 hours (150 ks) corresponding to about 30 orbits. Table 4 shows the a-posteriori error statistics (RMS) for the different LORF axes: total RMS is shown together with MBW and higher frequency components. Being a real-time estimate, low frequency dominates due to relevant components of the measurement errors which are integrated during the filter time constants, a fact that harmonic analysis, not treated here, had predicted.

Table 4. LORF error RMS [μrad]

Axis	Total (target)	MBW	HF
x	0.48 (200)	0.08	0.001
y	4.0 (200)	0.8	0.03
z	1.6 (200)	0.04	0.03

Total RMS in Table 4 is largely lower than target in Table 2, showing filter efficiency. Fig. 3 shows time history of the along-track error: the MBW component is much lower than the whole error as expected, being progressively attenuated by the filter narrow BW.

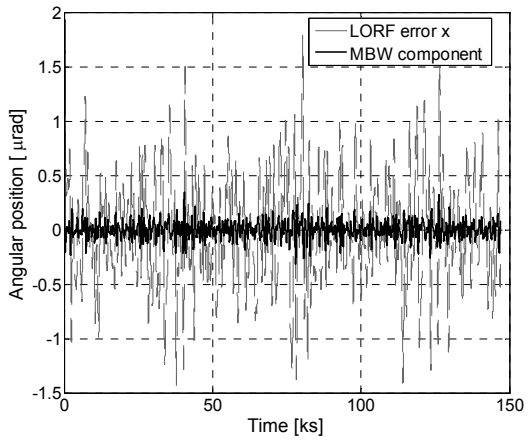

Fig. 3. LORF along-track error and MBW component (narrow strip).

Considerations regarding Fig. 3 are confirmed by the error PSD shown in Fig. 4 having a wide margin with respect to target bound. Out-of-plane and radial (lateral) components overlap, while along-track error appears much lower. The reason is due to residual non-gravitational accelerations, ideally zero in case of full drag-free control an each axis, actually non zero at lower frequencies along the lateral orbit movements for reasons of propellant saving.

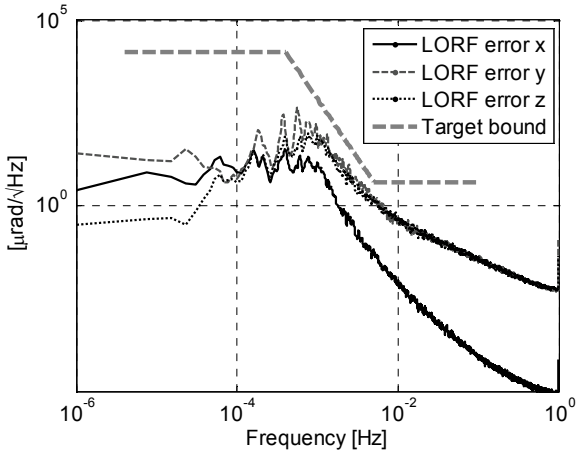

Fig. 4. LORF error PSD.

Fig. 4 shows the observer BW to approach 1 mHz, close to the mean orbit frequency f_O, because of measurement errors. Only accurate orbit and disturbance dynamics, as pursued in this paper, can cope with such a narrow BW and stability inequality (41).

Fig. 5 overlaps the pitch attitude with the corresponding LORF error. Two mission phases are shown: in the former one ending at about 80 ks, attitude is just measured by star trackers affected by noise and bias; in the latter, data fusion between payload accelerometers and star trackers allow cancelling high frequency noise: bias of course remains.

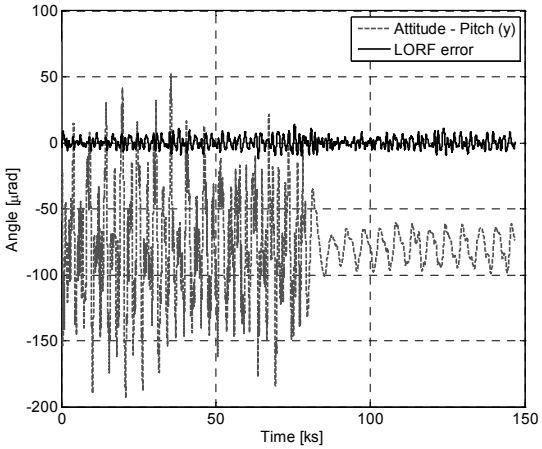

Fig. 5. Residual attitude and LORF error.

6. CONCLUSIONS

A state predictor for the real-time estimation of the local orbital frame of drag-free LEO satellites has been presented. It is designed as a predictor-corrector around the Embedded Model of orbit dynamics made by controllable and disturbance dynamics. Simulated results are compatible to GOCE target bounds with a good margin.

REFERENCES

Bertotti, B. and P. Farinella (1990) *Physics of the Earth and the Solar System*. Kluwer Academic Pu., Dordrecht.

Bisnath S. (2004) Precise orbit determination of Low Earth Orbiters with a single GPS receiver-based, geometric strategy. Ph.D. Dissertation, University of New Brunswick.

Canuto, E., P. Martella and G. Sechi G. (2003) Attitude and drag control: an application to the GOCE satellite. *Space Science Reviews*, **108** (1-2), 357-366.

Canuto, E. and A. Rolino (2004) Multi-input digital frequency stabilization of monolithic lasers. *Automatica*, **40** (12), 2139-2147.

Canuto, E. (2007a) Embedded Model Control: outline of the theory. *ISA Trans*. **46** (3), 363-377.

Canuto, E (2007b) Drag-free and attitude control for the GOCE satellite. *Automatica,* July 2008, in press.

Canuto, E (2007c) Drag-free control of the GOCE satellite: noise and observer design. Submitted to *IEEE Trans. on Control System Technology.*

Kaplan E.D. ed. (1996) *Understanding GPS: Principles and Applications.* Artech House Publishers, Boston.

Montenbruck O. and B. Gill (2000) *Satellite orbits, models, methods, application.* Springer-Verlag, Berlin.